Thermal conductivity profile determination in proton-irradiated ZrC by spatial and frequency scanning thermal wave methods

C. Jensen', M. Chirtoc, N. Horny, J. S. Antoniow, H. Pron, and H. Ban

Citation: Journal of Applied Physics **114**, 133509 (2013); doi: 10.1063/1.4821432

View online: http://dx.doi.org/10.1063/1.4821432

View Table of Contents: http://aip.scitation.org/toc/jap/114/13

Published by the American Institute of Physics

Thermal conductivity profile determination in proton-irradiated ZrC by spatial and frequency scanning thermal wave methods

C. Jensen,[1,2,a)] M. Chirtoc,[1] N. Horny,[1] J. S. Antoniow,[1] H. Pron,[1] and H. Ban[2]
[1]*GRESPI, Multiscale Thermophysics Lab., Université de Reims Champagne-Ardenne URCA, Moulin de la Housse BP 1039, Reims 51687, France*
[2]*Department of Mechanical and Aerospace Engineering, Utah State University, Logan, Utah 84322, USA*

(Received 25 June 2013; accepted 2 September 2013; published online 4 October 2013)

Using complementary thermal wave methods, the irradiation damaged region of zirconium carbide (ZrC) is characterized by quantifiably profiling the thermophysical property degradation. The ZrC sample was irradiated by a 2.6 MeV proton beam at 600 °C to a dose of 1.75 displacements per atom. Spatial scanning techniques including scanning thermal microscopy (SThM), lock-in infrared thermography (lock-in IRT), and photothermal radiometry (PTR) were used to directly map the in-depth profile of thermal conductivity on a cross section of the ZrC sample. The advantages and limitations of each system are discussed and compared, finding consistent results from all techniques. SThM provides the best resolution finding a very uniform thermal conductivity envelope in the damaged region measuring $\sim 52 \pm 2\,\mu$m deep. Frequency-based scanning PTR provides quantification of the thermal parameters of the sample using the SThM measured profile to provide validation of a heating model. Measured irradiated and virgin thermal conductivities are found to be $11.9 \pm 0.5\,\mathrm{W\,m^{-1}\,K^{-1}}$ and $26.7 \pm 1\,\mathrm{W\,m^{-1}\,K^{-1}}$, respectively. A thermal resistance evidenced in the frequency spectra of the PTR results was calculated to be $(1.58 \pm 0.1) \times 10^{-6}\,\mathrm{m^2\,K\,W^{-1}}$. The measured thermal conductivity values compare well with the thermal conductivity extracted from the SThM calibrated signal and the spatially scanned PTR. Combined spatial and frequency scanning techniques are shown to provide a valuable, complementary combination for thermal property characterization of proton-irradiated ZrC. Such methodology could be useful for other studies of ion-irradiated materials. © *2013 AIP Publishing LLC*. [http://dx.doi.org/10.1063/1.4821432]

I. INTRODUCTION

Ion-irradiated material studies provide valuable insight into material behavior under irradiation conditions that can be correlated to neutron irradiation effects.[1] The need for temporally and monetarily costly studies of neutron interaction with materials can potentially be mitigated. In general, the irradiation process is one of few tools available with the ability to alter material structure in such a way that it can be measured and correlated to the resulting effects on the material's properties. One of the challenges associated with studies of such materials is that the affected layer is typically very thin, ~0.1–100 μm for laboratory accelerators.[2,3]

Understanding thermal properties of nuclear as well as most any other engineering materials is vital for both science and application. Few investigations have been reported of ion-irradiation effects on thermal transport properties, in part, due to the challenge associated with measurements of the size of the zones of interest (~0.1–100 μm). General characteristics of the resulting damage profile from heavy ion irradiation are a very limited depth of penetration with a strongly peaked damage profile. For light-ions (protons), the irradiation-damaged profile can exceed several tens of microns with relatively low beam energies while maintaining a fairly constant damage level over most of the profile (for more detail about particle characteristics, see Ref. 3).

In recent years, frequency-based thermal wave methods have been used to investigate thermophysical properties of ion-irradiated samples.[4–6] In these techniques, periodic heating is applied to a sample inducing a periodic temperature response in the sample. Commonly, heating is by laser or other light source; thus, many methods are termed photothermal. The induced periodicity of the temperature field in the sample follows the mathematical description of evanescent waves, thus the term thermal wave. Different thermal wave techniques are distinguished by the methods used for exciting and detecting these thermal waves. The distance these thermal waves travel before the temperature amplitude decays to 1/e of the amplitude at the heated surface is called the thermal diffusion length, $\mu = (\alpha/\pi f)^{1/2}$, where α is material thermal diffusivity and f is the heating modulation frequency. Using the frequency-dependent thermal diffusion length, these techniques then have the advantage of non-destructively, depth-profiling the sample with knowledge of sample thermal and geometric parameters. For previous photothermal studies of ion-irradiated samples, numerically calculated irradiation-damage profiles have been used to approximate the profile as a discretely layered structure with thicknesses taken from the numerical predictions.[4,6] One study used transmission electron microscopy of the in-depth irradiation damage profile to validate the numerically predicted profile.[5]

Zirconium carbide (ZrC) has several potential applications in fuels for next generation nuclear reactors. Irradiation effects, especially the degradation of thermophysical properties, on ZrC are still poorly understood, especially in regard

a)Electronic mail: colby.jensen@aggiemail.usu.edu

to material types, irradiation conditions, and damaging doses relevant to its application. The physical properties of ZrC are highly dependent on stoichiometry. In the literature, ZrC has a room temperature thermal conductivity (k) ranging from 17–40 $W\,m^{-1}\,K^{-1}$ depending on stoichiometry and density.[7,8] Also, being a metal ceramic, ZrC has k comprised of the summed contributions of electrons and phonons (discussed in Sec. IV B 1). Favorable for the IR detection methods used in this work, ZrC has high emissivity (~0.9).[9]

Only a few studies have reported measurements of irradiation effects on thermal conductivity.[4,10,11] David *et al.* found a 50% and 75% decrease in thermal conductivity for two different dosages on ZrC (virgin $k = 20\,W\,m^{-1}\,K^{-1}$, composition not specified) irradiated by 25.8 MeV krypton ions.[4] Snead *et al.* found only minor degradation in k of ZrC with C/Zr ratio of 0.87, from exposure to fast neutron irradiation. The non-irradiated thermal conductivity for their sample was between 12 and 16 $W\,m^{-1}\,K^{-1}$. They attributed the reduction mainly to phonon scattering as the electronic contribution to thermal conductivity showed no change.[11]

The objective of this study is to characterize the thermal conductivity degradation in proton-irradiated ZrC. In a manner not previously studied, four thermal wave methods are used in this work to characterize the proton-irradiated layer in ZrC including scanning thermal microscopy, spatial-scanning front-detection photothermal radiometry (PTR), lock-in IR thermography (lock-in IRT), and tomographic, frequency-based PTR. A full mathematical description of the sample is presented with reduced forms for special cases related to (1) various limits in frequency scanning PTR and (2) each of the spatial scanning techniques. The profiles obtained by each of the spatial scanning methods are compared to each other and the numerical prediction of the ion-damage profile. For the frequency-scanned PTR measurements, a sample of undamaged ZrC material was used first to measure the thermal properties of the virgin material. The virgin material properties and spatially scanned profile allow for the irradiation-damaged zone thermal properties to be calculated from measurement on the irradiated ZrC sample. The complementary nature of the various techniques validates the measured profile and the measured degradation of thermal conductivity in the ZrC sample.

II. SAMPLE DESCRIPTION

In this work, a 3 mm disc of nearly stoichiometric (C/Zr = 1.01), hot-pressed, commercial-grade zirconium carbide (ZrC) was cut from a rod having a measured density of 6.58 $g\,cm^{-3}$, near the theoretical density of 6.64 $g\,cm^{-3}$. The value of specific heat, c_p, has been taken from the literature as 368 $J\,kg^{-1}\,K^{-1}$.[7,12,13] One face of the 500 μm thick disc was polished and irradiated using 2.6 MeV proton beam. Both before and after irradiation the sample grain size was studied using scanning electron microscopy (SEM) finding an average size of 24 μm and no indication of grain boundaries, respectively. A more complete description of the irradiation preparations and conditions of the sample is given by Yang *et al.*[14]

Proton irradiation was performed at 600 °C until the damage level reached an approximate level of 1.75 dpa (displacements per atom) in the nearly constant portion of the profile comprising the first several tens of microns of the damage depth profile. The damage profile calculated by TRIM2008 (Ref. 15) (transport of ions in matter) using threshold displacement energies of 35 eV for zirconium and 25 eV for carbon as given by Yang *et al.*[14] is shown in Fig. 1(a). The numerical result is compared to the profiles obtained using thermal transport measurement techniques in Sec. IV A. The damage profile will have some proportionality to the degradation of thermal conductivity of the material.

After irradiation, a fragment of the sample was fractured off to reveal the cross section of the damage profile to measure using the spatial scanning techniques. The cross section was mounted in epoxy and polished down to 0.02 μm colloidal silica. The remaining disc was used for the frequency-based PTR measurements. Sample measurement configurations are shown in Fig. 1(b). Additionally, a disc of undamaged ZrC was used to measure the thermal properties of the virgin ZrC material.

III. MEASUREMENT METHODS AND THEORY

A. Scanning thermal microscopy (SThM)

SThM[16–18] was used to measure the thermal conductance profile of the cross-sectioned, irradiated ZrC sample. The SThM measurements were made using a Wollaston-type thermoresistive probe mounted on a TA Instruments μTA 2990 Micro-Thermal Analyzer in constant temperature mode. In this mode, the measured power is then directly proportional to the thermal conductance of the tip to the sample. Assuming similar physical contact characteristics for a given probe provides the ability to extract information regarding the thermal conductivity of the sample.[19] The lateral resolution is determined by the size of

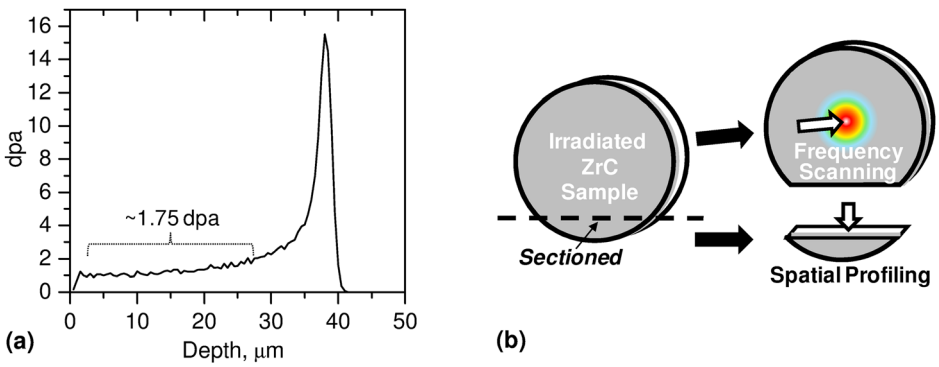

FIG. 1. (a) Numerically calculated damage profile for 2.6 MeV protons in ZrC from TRIM2008.[13] (b) Sample measurement configurations for frequency and spatial profiling techniques.

tip-sample contact area. This statement is valid also when the SThM is operated in the ac mode and is known as the super-resolution effect of thermal wave probing.[20] It is due to the fact that the thermal diffusion length in the sample at the used modulation frequencies (up to tens of kHz) is still much larger than the size of the contact area. The ac and dc modes provide the same information about the sample. Therefore, active (sample heating), single-tip SThM measurement is not a true thermal wave method in the sense that probing (heating) depth is not controlled by heating modulation frequency.

Quantitative measurement results for thermal conductivity are prone to large uncertainties due to reproducibility of the tip contact and decreasing measurement sensitivity for medium-to-high thermal-conductivity samples (k_{ZrC}). As a consequence, SThM functions well to measure relative values, especially within a single scan line where thermal contact conditions change little. The irradiated-ZrC cross-section is a good sample for measuring relative k values because of similar physical characteristics between the damaged and virgin zones that can be scanned in a single line.

B. Lock-in IRT

For the lock-in IRT measurements,[21–23] the same laser/acousto-optical modulator (AOM) used in the PTR setup (described in III C 1) was used to heat the surface of the cross section of the sample at a frequency of 40 Hz. An IR (wavelength 3.5–5.0 μm) camera model (CEDIP Titanium) with a frame rate of 100 Hz recorded the periodic heating response of the sample over a period of 10 s. Home-made software (CAMIR) was used to calculate the amplitude and phase for each pixel, at the heating frequency, using lock-in techniques. Figure 2(a) shows a schematic of the measurement setup. The result is both amplitude and phase images of the entire sample.

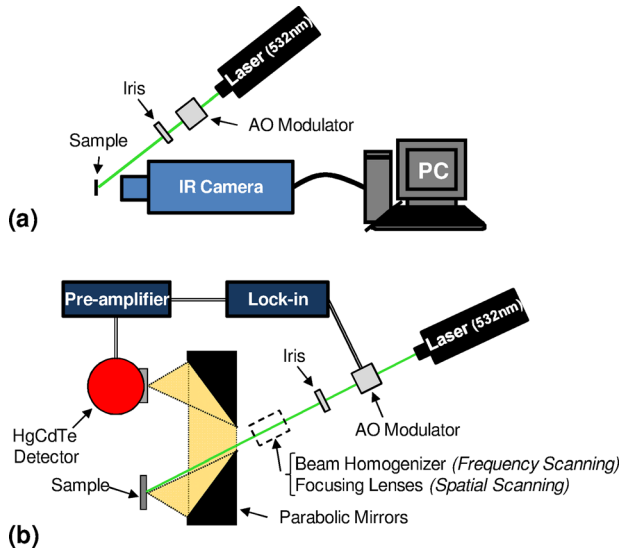

FIG. 2. Schematics of measurement systems: (a) lock-in infrared thermography (IRT) and (b) front-detection photothermal radiometry (FD-PTR) used for frequency and spatial scanning.

C. PTR

1. PTR method with periodic excitation

A schematic of the PTR[24–26] system in front detection configuration (FD-PTR), used for both spatial and frequency scanning, is presented in Fig. 2(b). The system uses a DPSS, 532 nm laser modulated by an AOM at a given frequency to heat the sample surface. Parabolic mirrors capture the emitted IR radiation from the sample, focusing it into an HgCdTe detector with a 1 mm^2 detection area. A preamplifier passes the signal from the detector to a lock-in amplifier which measures the temperature amplitude and phase relative to the heat source. The results were normalized using the electro-optical transfer function of the setup at low frequencies. For higher frequencies (>10 kHz), normalization was performed using data from polished steel.

For the frequency scanning measurements, the Gaussian heating laser beam profile was homogenized using a flat-top beam shaper. In this way, the entire surface of the sample (<3 mm diameter) was heated uniformly, creating an approximate 1D heating condition. Measured amplitude and phase spectra for the range of frequencies having the greatest sensitivity to the parameters of interest (Sec. III C 3) were then used to fit the thermal model (Sec. III C 2) to extract the measured parameters.

For the spatial scanning measurements, the flat-top beam shaper was replaced with a set of lenses to focus the heating spot to a size of ≈50 μm. The sample was then scanned laterally using a micrometer stage.

2. Frequency scanning PTR response of a two-layer sample

As with other works, the continuously varying damage in the irradiated zone (see Fig. 3) is approximated as a multilayered structure.[4–6] As compared to other types of ions, proton irradiation lends particularly well to a structure approximated by discrete layers due to the relatively thick and uniform damage level spanning most of the damaged zone in the sample. From the measured profile obtained from SThM measurements,[19] the proton-irradiated ZrC sample is modeled as a homogeneous damaged layer on the bulk, virgin ZrC material as seen in Fig. 3. An interfacial thermal resistance, R_{th}, is placed between the two materials to account

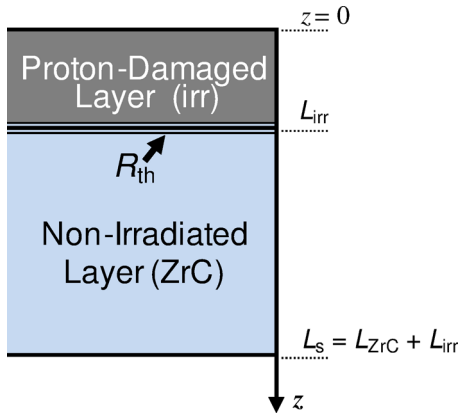

FIG. 3. Schematic of heat model geometry used for frequency-scanning FD-PTR for irradiated ZrC sample.

for the possibility of a greater damaged zone, seen in the numerically calculated damage profile and/or the presence of void space at the interface (discussed in more detail in Sec. IV B 2). The later discussed spatial profiling measurements showed no evidence of a secondary layer; however, for a thin layer, using R_{th} is also mathematically appropriate.

Several models for multilayer systems with modulated heating have been developed.[27,28] In this work, the thermal quadrupoles method has been used to model the irradiated ZrC sample.[29] The sample is considered adiabatic (heat losses neglected) and opaque to the 532 nm laser heat source (absorption calculated from the dielectric constant of $ZrC_{0.96}$ results in a penetration depth of <50 nm). In the simplified case of the ZrC sample under plane illumination (1D), a matrix relationship between the temperature and heat flux at the front and at the rear of the sample may be found as

$$\begin{pmatrix} T_{irr}(z=0) \\ \varphi_{irr}(z=0) \end{pmatrix} = \begin{pmatrix} A_{irr} & B_{irr} \\ C_{irr} & D_{irr} \end{pmatrix} \cdot \begin{pmatrix} 1 & 1 \\ 1 & R_{th} \end{pmatrix} \cdot \begin{pmatrix} A_{ZrC} & B_{ZrC} \\ C_{ZrC} & D_{ZrC} \end{pmatrix} \cdot \begin{pmatrix} T_{ZrC}(z=L_s) \\ \varphi_{ZrC}(z=L_s) \end{pmatrix}, \tag{1}$$

where $A_i = D_i = \cosh(\sigma_i \cdot L_i)$, $Bi = \sinh(\sigma_i \cdot L_i)/(k_i \cdot \sigma_i)$, $C_i = k_i \cdot \sigma_i \cdot \sinh(\sigma_i \cdot L_i)$ for layer "i." σ_i is the complex thermal wave vector, $\sigma_i = (i\omega/\alpha_i)^{1/2} = (1+i)/\mu_i$, where $\mu_i = (\alpha_i/\pi f)^{1/2}$ is the thermal diffusion length. The depth sensitivity controlled by μ makes frequency-based thermal-wave techniques powerful for non-destructively probing the in-depth properties of materials. $\alpha_i = k_i/(\rho_i \cdot c_{pi})$ is thermal diffusivity with thermal conductivity, k_i, density, ρ_i, and specific heat capacity, c_{pi}, for material "i." The term "$k_i \cdot \sigma_i$" may be simplified to $e_i \cdot (i \cdot \omega)^{1/2}$ where $e_i = (k_i \cdot \rho_i \cdot c_{pi})^{1/2}$ is the thermal effusivity.

Assuming the heat losses at the rear are negligible so that $\varphi_{ZrC}(z = L_s) = 0$, the thermal impedance of the sample in a front detection configuration (FD-PTR) may be found as

$$Z_{irrZrC} = \frac{T_{irr}(z=0)}{\varphi_{irr}(z=0)} = \frac{A_{irr} \cdot A_{ZrC} + B_{irr} \cdot C_{ZrC} + A_{irr} \cdot C_{ZrC} \cdot R_{th}}{C_{irr} \cdot A_{ZrC} + D_{irr} \cdot C_{ZrC} + C_{irr} \cdot C_{ZrC} \cdot R_{th}}, \tag{2}$$

or in an explicit form as

$$Z_{irrZrC} = \frac{1-i}{e_{irr}\sqrt{2\omega}} \times \frac{1 + (e_{ZrC}/e_{irr})\tanh(\sigma_{irr}L_{irr})\tanh(\sigma_{ZrC}L_{ZrC}) + \sqrt{i\omega}e_{ZrC}R_{th}\tanh(\sigma_{ZrC}L_{ZrC})}{\tanh(\sigma_{irr}L_{irr}) + (e_{ZrC}/e_{irr})\tanh(\sigma_{ZrC}L_{ZrC}) + \sqrt{i\omega}e_{ZrC}R_{th}\tanh(\sigma_{irr}L_{irr})\tanh(\sigma_{ZrC}L_{ZrC})}. \tag{3}$$

At low frequencies the whole sample is thermally thin ($L_{irr}/\mu_{irr} \ll L_{ZrC}/\mu_{ZrC} \ll 1$). The thin irradiated layer can be incorporated in the bulk, and in a first approximation Eq. (3) yields

$$Z_{ZrC} = -i/(\omega L_s \rho_s c_{ps}), \tag{4}$$

meaning that the PTR signal amplitude is $\propto f^{-1}$ and the phase is $-90°$. There is no influence from the parameters of the irradiated layer or from R_{th}. The sample is equivalent to the homogeneous bulk ZrC.

At intermediate frequencies the bulk ZrC is thermally thick ($L_{irr}/\mu_{irr} \leq 1 \ll L_{ZrC}/\mu_{ZrC}$). Then $\tanh(\sigma_{ZrC}L_{ZrC}) \approx 1$ and Eq. (3) reduces to

$$Z_{irrZrC} = \frac{1-i}{e_{irr}\sqrt{2\omega}} \frac{1 + (e_{ZrC}/e_{irr})\tanh(\sigma_{irr}L_{irr}) + \sqrt{i\omega}e_{ZrC}R_{th}}{\tanh(\sigma_{irr}L_{irr}) + (e_{ZrC}/e_{irr}) + \sqrt{i\omega}e_{ZrC}R_{th}\tanh(\sigma_{irr}L_{irr})}. \tag{5}$$

This frequency range offers the most information on the irradiated layer. Referring to the bulk layer, Eq. (5) contains only its effusivity, e_{ZrC}.

At high frequencies both layers become thermally thick ($1 \ll L_{irr}/\mu_{irr} \ll L_{ZrC}/\mu_{ZrC}$), and Eq. (5) further simplifies to

$$Z_{irr} = (1-i)/(e_{irr} \cdot \sqrt{2\omega}), \tag{6}$$

meaning that the amplitude is $\propto f^{-1/2}$ and the phase is $-45°$. The only accessible parameter is e_{irr}, via the amplitude. There is no influence from the bulk layer. Equation (6) is applicable for the spatial-scanning PTR on very shallow depths. It allows measuring relative effusivity variations over the sample cross-section.

Depending on boundary conditions, a layer manifests either its capacitive impedance component Z_C (like Eq. (4)) under quasi-isothermal conditions or its resistive component $R = L/k$ under temperature gradients between the two faces. In the quadrupole formalism the two components appear in parallel. As long as $Z_C \gg R_{th}$, Z_C can be neglected and L can be set to zero. In a multilayer system, such layer can be replaced by an interfacial thermal resistance R_{th} having the same value as R. Note that the condition for this equivalence depends on frequency. In Sec. IV B 2 it will be shown that this condition is fulfilled in the present study.

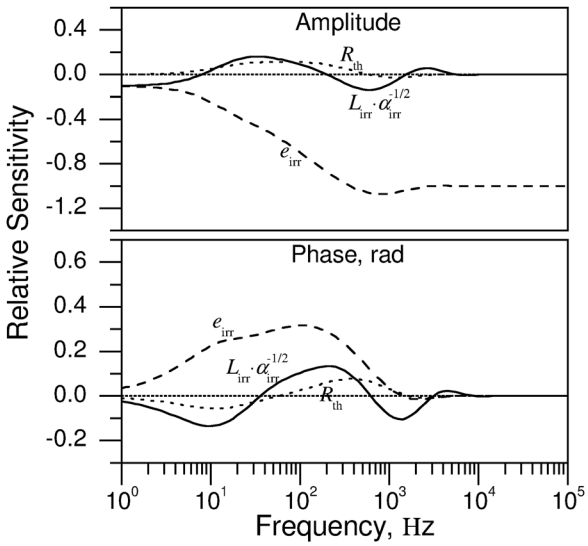

FIG. 4. Relative sensitivities of the (top) amplitude and (bottom) phase to independent parameters for proton-irradiated ZrC using the values for parameters shown in Table II.

3. Sensitivity analysis

From the theoretical model presented above, the dependence of the complex impedance to ω is a function of five independent parameters: $L_{irr}\alpha_{irr}{}^{-1/2}$, $L_{ZrC}\alpha_{ZrC}{}^{-1/2}$, e_{irr}, e_{ZrC}, and R_{th}. The parameters related to the virgin material are measured independently so that the independent parameters to be determined are $L_{irr}\alpha_{irr}{}^{-1/2}$, e_{irr}, and R_{th}. To ensure unique fitting results, the relative sensitivity of the thermal parameters to be fitted has been studied. The relative sensitivity of a function, $F(p)$, to parameter p is defined as

$$S_p = \frac{\partial F/F}{\partial p/p} = \frac{\partial(\ln F)}{\partial(\ln p)}. \tag{7}$$

In the case of complex quantities, $F = A\cdot\exp(i\varphi)$, it can be shown that $S_p = S_{A,p} + iS_{\varphi,p}$, where $S_{\varphi,p} = \partial\varphi/\partial(\ln p)$.[30]

A value $S_{A,p} = -1$ implies $F \propto p^{-1}$. The relative sensitivities for A and φ to the three parameters related to the irradiated layer are plotted in Fig. 4. Their sensitivity spectra are different indicating that the respective parameters are not correlated. Therefore, the fit of this parameter set is feasible. Moreover, the features of the spectra are consistent with the discussion of Eqs. (4)–(6). At low frequency there is practically no sensitivity to the plotted parameters (Eq. (4)) while at high frequency there is only amplitude sensitivity to e_{irr} ($S_{A,eirr} = -1$) as predicted by Eq. (6). All three parameters reveal strongest sensitivity from 8 Hz to 8 kHz providing the range of frequencies selected for fitting them in the thermal model to the FD-PTR results. This range encompasses the more restrictive interval of 17.5–580 Hz set by the thermally thin-thick limits of the two layers (see Fig. 6 and Table II). The parameter of interest k_{irr} is embedded in $L_{irr}\alpha_{irr}^{-1/2}$ and in e_{irr}. It will be eventually determined using other complementary data (see Sec. IV B 2).

IV. RESULTS AND DISCUSSION

Results are first presented for the spatial scanning methods as the obtained profiles will contribute to the model used in extracting the thermal parameters from the frequency scanned FD-PTR results. Each of the spatial measurements was performed on the polished cross-section of the irradiated ZrC sample. To ensure unique fitting results for the damaged layer of ZrC, an undamaged ZrC sample was first measured using frequency-scanned FD-PTR to obtain thermal parameters for the virgin material. The FD-PTR measurements were then made on the irradiated face of the remaining piece of the ZrC sample, from which the thermal properties of the irradiated layer were calculated.

A. Spatial scanning

The results for the three spatial scanning techniques are presented in Figs. 5(a)–5(c). In all cases, depth = 0 μm corresponds to the irradiated surface of the ZrC cross section. Figure 5(a)

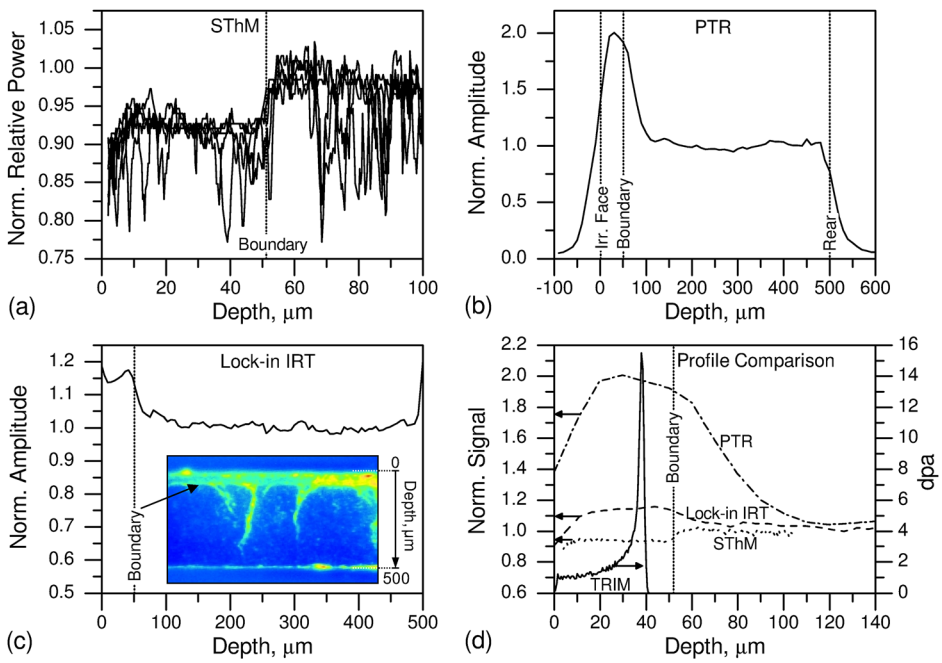

FIG. 5. Spatially scanned profiles of irradiated-ZrC cross-section. Vertical line "Boundary" marks SThM measured thickness of irradiated layer in (a)-(d). (a) Several SThM profiles used to piece together overall profile (upper levels). (b) PTR amplitude profile at 1 MHz heating with 50 μm focused spot. (c) Average of four lock-in IRT profiles at 40 Hz heating of entire cross section, taken from amplitude image (inset, amplitude image showing sample cross section). (d) Comparison of measurements from spatial scanning techniques (edge effects removed in lock-in IRT) and numerical prediction of damaged layer.

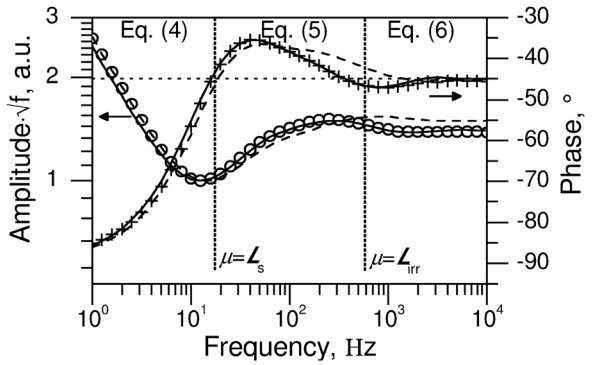

FIG. 6. FD-PTR amplitude and phase for proton-irradiated ZrC. Points, experiment; solid lines, fit with Eq. (3) and $L_{irr}\alpha_{irr}^{-1/2}$, e_{irr}, and R_{th} as free parameters; dashed lines, Eq. (3) with $R_{th}=0$. Key parameter values are listed in Table II. The thermally thin-thick vertical markers (f_T given in Table II) delimit three frequency sub-ranges and the respective theoretical special cases.

shows several SThM measured profiles extracted from a constant temperature scanned image. The resulting measured profile has characteristics related to the specific thermal probe used in the measurements due to the differences in probes from the individual, hand fabrication process. As is more fully detailed in a previous work,[19] the true thermal conductivity profile for this probe was found to be the upper levels of the measured signal where the various dips were related to topographical effects of the surface. Clearly, the upper level represents a more stable, repeatable, and level envelope. Near the irradiated surface (depth $=0\,\mu$m), the decrease of signal is most likely due to an increasingly rounded edge (from polishing), changing tip-sample contact and not from a change of thermal properties.

Characteristic effects of the proton irradiation on the thermal conductivity of the sample are evident in the nearly flat and constant damaged region leading to a sharp transition from irradiation penetration depth to the virgin material.[3] Previously, using the combination of topographic and thermal images with validation from optical micrographs, the depth of irradiated/virgin transition was measured to be $52\pm2\,\mu$m.[19] The measured length corresponds to the front surface to the middle of the transition region while the uncertainty corresponds to the length of the transition region, $\sim4\,\mu$m. Also of significance and disagreeing with the numerical prediction, the profile reveals no evidence of greater degradation of k near the stopping range of the protons. Therefore, no intermediary layer of higher damage is assumed in the thermal model used for fitting PTR data. A previous work detailing the calibration of the SThM signal found $k_{irr}=10\pm2.4\,\mathrm{W\,m^{-1}\,K^{-1}}$ and $k_{ZrC}=30\pm10\,\mathrm{W\,m^{-1}\,K^{-1}}$.[19]

Figure 5(b) presents the normalized amplitude profile across the entire thickness of ZrC cross section measured by PTR with a focused laser heating spot of $\sim50\,\mu$m. The profile is normalized to the average value of the amplitude in the non-irradiated zone of the sample and represents the average of three spatial scans with a heating modulation frequency of 1 MHz. At this frequency $\mu\sim1$–$2\,\mu$m, meaning thermally thick sample heating case so that the amplitude is inversely $\propto e$ (Eq. (6)), assuming that the irradiated and non-irradiated zones have similar radiation properties. Although the diffusion length is small in this case, the limitation of lateral resolution was found to be the spot size, which was measured to be $\sim50\,\mu$m (at $1/e^2$) using a DataRay WinCamD profilometer. In the measured profile, the edges of the sample and the boundary between irradiated and non-irradiated zones evidence the insufficient resolution by gradual changes of signal representing a convolution of the laser spot across the two zones. The peak in the measured profile again shows the damaged layer, a zone of lower e ($e_{irr}<e_{ZrC}$).

Because the amplitudes are approximately $\propto e^{-1}$, the normalized profile should also represent the ratio of e_{ZrC} to the local thermal effusivity of the sample. In the damaged layer, a normalized peak of 2 represents the ratio e_{irr}/e_{ZrC}. Assuming the same volumetric heat capacity, this means that the conductivity ratio of the k_{ZrC}/k_{irr} is about 4. The width of the zone is wholly consistent with the measured width found in the SThM profile taking into consideration the heating spot size.

The final direct measurement of the thermal conductivity profile is displayed in Fig. 5(c) using lock-in IRT. The amplitude image of the ZrC sample from which the profiles were extracted is shown in the inset of the figure. Again, the resulting average of four profiles has been normalized to the level of the virgin ZrC. For this measurement, the heating frequency was limited to 40 Hz, giving μ of the order of L_s. For this reason the spatial resolution of the thermal signal is not as good as the pixel resolution of the camera, which was found to be approximately $5\,\mu$m. Also, for the same reason, any quantitative interpretation is more difficult to extract from the measurement. The normalized amplitude peak of ~1.2, much less then the PTR result, is expected due to the increased heat spreading due to the large thermal diffusion length whereas the PTR measurement is confined to a depth of ~1–$2\,\mu$m from the surface. Still, the damaged layer is clearly present with an apparent thickness of the order of $\sim50\,\mu$m.

A direct comparison of the three different spatial profiles along with the numerically calculated profile is found in Figure 5(d). In this figure, edge effects were removed in the lock-in IRT profiles by subtracting the mirror-inverted, non-irradiated edge from the irradiated edge profile. The SThM profile is represented by an average of the upper levels of the various profiles, considered to be the thermal conductivity profile of the sample. Table I summarizes the characteristics

TABLE I. Characteristics of thermal conductivity profiling methods used on proton-irradiated ZrC.

Method	Scanning type	Lateral resolution	Probing depth	k_{irr} ($\mathrm{W\,m^{-1}\,K^{-1}}$)	k_{ZrC} ($\mathrm{W\,m^{-1}\,K^{-1}}$)
SThM	Spatial	$\sim$Contact radius $\sim1\,\mu$m	$\sim$Contact radius $\sim1\,\mu$m	10 ± 2.4	30 ± 10
Lock-in IR Thermography	Spatial	Pixel size $=5\,\mu$m, $\mu\sim300\,\mu$m	$\mu\sim300\,\mu$m	…	…
PTR	Spatial	Heating spot size $\sim50\,\mu$m	$\mu\approx1$–$2\,\mu$m	$(1/4)\cdot k_{ZrC}$	…
PTR	Frequency	Measured spot size ~1 mm	$\mu\approx1\,\mathrm{mm}-1\,\mu$m	11.9 ± 0.5	26.7 ± 1

of each technique's measured profile. The SThM measurement has the best lateral resolution of the three methods and is, therefore, the most accurate for predicting the irradiation-induced damaged depth (used in Fig. 5). For the PTR and lock-in IRT, each has both a strength and a weakness concerning spatial resolution of the measurement that is each other's opposite. The PTR can operate at high frequencies (at the cost of reduced amplitude, $A \propto f^{-1/2}$) allowing for small μ, but the heating spot size used in this measurement is large relative to the needed resolution for measuring L_{irr}. Lock-in IRT has good spatial resolution, but frame rate limits the possibility of decreasing μ. For decreasing heating spot size, PTR resolution will have the inherit limitation from the IR wavelengths involved in detection (8–12 μm) as well as the conflict of diminishing IR signal vs. excessive sample heating.

In regards to the extraction of quantitative information, none of the spatial profiling methods used provide a reliable extraction of k. The value extracted for k_{ZrC} is at the upper limit of typical SThM sensitivity, and thus uncertainty becomes increasingly large for this range. For the PTR spatial scans, ratio of effusivities was extracted although again with large uncertainty, primarily related to the variations of thermal radiation properties (optical reflectivity and IR emissivity) across the sample surface. Still, the high emissivity ($\sim$0.9)[9] of ZrC is favorable for such analysis especially comparing between two zones of the "same" material. The results extracted from SThM and PTR are comparable and especially interesting when viewed from the perspective of measurement probing depth in the two measurements. For the PTR at 1 MHz heat modulation and the SThM, the probing depths are both on the order of a few microns. Therefore, the effects of the (larger) grain boundaries in the material are not measured. As was previously described, the irradiated zone shows no evidence of grain boundaries while the virgin ZrC is characterized by grain of $\sim$25 μm size. The virgin material would be expected to have a higher measured thermal conductivity (excluding longer scale effects due to boundary thermal resistance). Assuming $k_{\text{irr}} \sim 10\,\text{W m}^{-1}\,\text{K}^{-1}$, a value of $k_{\text{ZrC}}/k_{\text{irr}} = 4$ is not unreasonable for this measurement.

B. Frequency scanning

Equation (3) describes the thermal impedance of the ZrC sample, which is proportional to the sample surface temperature measured by the PTR system. The sensitivity analysis showed that the parameters, $L_{irr}\alpha_{irr}^{-1/2}$, e_{irr}, and R_{th}, are decorrelated and can be simultaneously fitted. Prior to that, the other two parameters $L_{ZrC}\alpha_{ZrC}^{-1/2}$ and e_{ZrC} were determined from a sample of undamaged ZrC material. Both amplitude and phase data were used for extracting the thermal parameters of interest. However, because the amplitude is dependent on instrumental factors, only relative values were used.

1. Thermal diffusivity of virgin ZrC

A non-irradiated sample of ZrC with known thickness L'_{s} was used to measure its thermal diffusivity from frequency-scanning FD-PTR. The direct transition between Eqs. (4) and (6) (with e_{ZrC} replacing e_{irr}) occurs at frequency f_T when $\mu_{ZrC} = L'_{\text{s}}$, whence $L'_s\alpha_{ZrC}^{-1/2} = (\pi f_T)^{-1/2}$. The PTR obtained spectrum and the f_T marker are similar to Fig. 6 below $\sim$100 Hz. Next the measured value of ρ and the literature value of c_{p} (see Sec. II) were used to extract k_{ZrC}. The result is a bulk value of $k_{\text{ZrC}} = 26.7 \pm 1\,\text{W m}^{-1}\,\text{K}^{-1}$ (Tables I and II). For comparison, thermal conductivity of ZrC reported in the literature varies from 17 to 40 $\text{W m}^{-1}\,\text{K}^{-1}$.[7,8,31–33] Finally, e_{ZrC} could also be determined. Using electrical resistivity values of 65–75 $\mu\Omega$ cm from the literature for similar stoichiometry ($\sim$1) and hot-pressed ZrC,[7,8] the Wiedemann-Franz Law predicts an electronic contribution to k of $\sim$9–11 $\text{W m}^{-1}\,\text{K}^{-1}$.

2. k_{irr} and R_{th}

Frequency scanning FD-PTR measurements were made on the irradiated face of the ZrC sample. Multiple measurement spectra were obtained over the span of a few months finding very consistent results. Amplitude (A) and phase (φ) results measured on the irradiated face of the ZrC sample along with the model results (Eq. (3)) are presented in Fig. 6. A summary of key parameter values are found in Table II. For visual purposes, the amplitude data are plotted as $A \cdot f^{1/2}$. This subtracts the overall amplitude slope of $f^{-1/2}$ found in the pre-factor of Eq. (3). At low frequencies, the results are characteristic of a thermally thin sample ($\mu > L_{\text{s}}$), where A demonstrates f^{-1} dependence and φ approaches $-90°$ (cf., Eq. (4)). For high frequencies ($\mu < L_{\text{s}}$), $A \cdot f^{1/2}$ is flat while $\varphi \to -45°$ (cf., Eq. (6)). The dashed lines are plots of Eq. (3) for $R_{\text{th}} = 0$. The differences relative to the full model are relatively small in the mid-frequency range and vanish outside this range. This behavior is consistent with the low sensitivity spectra to R_{th} from Fig. 4.

The simultaneous fit of the independent parameters: $L_{irr}\alpha_{irr}^{-1/2}$, e_{irr}, and R_{th} to A, and φ with Eq. (3) provides the results shown in Table II. Using the measured values of L_{irr}, from α_{irr} and e_{irr}, results in $k_{\text{irr}} = 11.9 \pm 0.5\,\text{W m}^{-1}\,\text{K}^{-1}$ and $(\rho \cdot c_{\text{p}})_{\text{irr}} = (2.42 \pm 0.1) \times 10^6\,\text{J m}^{-3}\,\text{K}^{-1}$. The fit value of interfacial resistance is $R_{\text{th}} = (1.58 \pm 0.1) \times 10^{-6}\,\text{m}^2\,\text{K W}^{-1}$. k_{irr} is dependent on L_{irr} of the sample due to the parameter dependency of the model. The resulting value of $(\rho \cdot c_{\text{p}})_{\text{irr}}$ is nearly identical to the value of the non-irradiated material.

TABLE II. Key sample parameters derived from independent fit parameters ($L_{irr}\alpha_{irr}^{-1/2}$, e_{irr}, and R_{th}) and from additional measurements: m denotes previously measured, SThM denotes SThM measurement, PTR denotes FD-PTR measurement. Transition frequencies f_{T} for thermally thin-thick ($\mu = L$) irradiated and bulk layers are also given.

Layer	f_T (Hz)	L (μm)	k ($\text{W m}^{-1}\,\text{K}^{-1}$)	$\rho c_{\text{p}} \cdot 10^{-6}$ ($\text{J m}^{-3}\,\text{K}^{-1}$)	$R_{\text{th}} \cdot 10^6$ ($\text{m}^2\,\text{K W}^{-1}$)
Bulk ZrC	17.1	453 ± 2 (SThM & m)	26.7 ± 1 (m)	2.42 (lit)[7,12]	
Irr. ZrC	579	52 ± 2 (SThM)	11.9 ± 0.5 (PTR)	2.42 ± 0.1 (PTR)	1.58 ± 0.1 (PTR)

Irradiation effect on heat capacitance is not expected to be great, and for a similar material, SiC was found to be practically non-existent for neutron irradiation.[34] As further validation, image analysis was performed on an optical micrograph of the sample cross section (e.g., Fig. 7). Comparing the number of pixels related to defect areas (appear porous) between the two zones indicates a 5% possible density change (decrease). This result validates the fit procedure. The irradiation-induced degradation of k is then ~55%. Previously, using an SThM signal calibration, k_{irr} was found to be $10 \pm 2.4\,W\,m^{-1}\,K^{-1}$ while the k_{ZrC} was $30 \pm 10\,W\,m^{-1}\,K^{-1}$ (Table I in Ref. 19), comparing favorably with the present PTR measurements. The SThM-measured k_{ZrC} showed relatively more variability that was attributed to both decreased sensitivity and the localized measurement, not capturing longer scale effects such as grain boundaries. However in the irradiated zone the dominant mechanism of thermal transport degradation is a high concentration of nanometer-sized Frank loops that would be manifest in both SThM and PTR. Grain boundaries were not found in the irradiated zone of the ZrC sample.[14]

Clarke[35] developed a model to estimate the minimum k for a material in an amorphous state at high temperatures. The model only accounts for acoustic phonon modes and is formulated based on expressions for minimum phonon mean free path and mean phonon velocities. The mean free path is formulated from the cube root of the volume of a molecule. Using this expression, the minimum calculated thermal conductivity, k_{min}, of ZrC is $1.6\,W\,m^{-1}\,K^{-1}$. Snead *et al.* found little change of electrical resistivity in ZrC resulting from fast neutron irradiation. The small changes of thermal conductivity were then attributed to phonon scattering from irradiation-induced defects.[11] While no measurements of electrical resistivity were made in this work for comparison, assuming the change of the electronic contribution to k is relatively small as is common in ceramic material,[36] the measured k_{irr} compared to the electronic contribution calculated in Sec. IV B 1 evidences a drastic reduction of the phonon contribution of k, to the order of k_{min}.

From R_{th} and an approximate thickness for the secondary layer as 5 μm from the TRIM profile, k for such a layer would be approximately $L/R_{th} = 3.2\,W\,m^{-1}\,K^{-1}$, comparable to what others have found for k of regions of peak damage.[4,5] On the other hand, the capacitive impedance Z_C of the same layer satisfies the condition $Z_C \gg R_{th}$ for frequencies up to 8.3 kHz. The sensitivity of PTR method to R_{th} is situated below this frequency limit, and therefore the effect of R_{th} is indistinguishable from that of an equivalent 5 μm thick layer (see Sec. III C 2). With the other methods, the spatial profiles made of the irradiation-damaged profile reveal no evidence of a region of peak damage (sharp degradation of k). Although in such a configuration, the excitation thermal gradients are oriented primarily parallel to the interface, which is unfavorable for the detection of R_{th}. Yet, from the frequency-based FD-PTR measurements, the shape of the profiles shows the existence of a strong resistance at the rear of the irradiated layer. One theory to explain this resistance is that it may not actually be due to the damaged microstructure as suggested by the TRIM results. Instead, evidence supports the possibility of small voids in the material that have been pushed by the proton irradiation to congregate at the backside of the damaged zone.

Figure 7 shows an optical micrograph of the sample cross-section, in which the damaged layer is apparent. In the micrograph, the polished sample has many "defect" structures (void space based on topographic measurements from SThM) that appear as dark regions. The irradiated layer is clearly visible due to less defects and a higher concentration of defects at the rear of the layer. In some regions, "crack"-like structures are visible, running primarily perpendicular to the irradiated surface. All of these "cracks" (appear to be aligned void space, originating from the material formation process), terminate at the backside of the irradiated zone. For some, they have the appearance of being bent into the plane of the backside of the irradiated layer. In the extreme case, the irradiated layer completely delaminated off the bulk layer after accidental mechanical stress was applied to the sample.

Similar effects were documented in a study of proton-irradiated ZrN, where they hypothesized that voids in the material had been moved through the material by the proton beam front and coalesced at the peak of the damage profile.[37] The result was transgranular cracking with void surfaces having silicon rich oxides. No composition analysis was performed on the ZrC sample studied here. Although the SThM measurements found the defect regions to be of lower thermal conductance, even though such "hole"-like regions would typically increase contact surface area with the thermal probe, indicative of lower conductivity material such as oxides.

Further support of the non-existence of a region of peak damage of the material microstructure as seen in the TRIM results can be inferred from molecular dynamics simulations done by Brutzel *et al.*[38] Their simulations of collision cascades found that point defects are primarily created while no amorphization was observed. Yang *et al.* showed consistent findings with this ZrC sample in an experimental study, with no evidence of amorphization, but high concentrations of nanometer-sized Frank loops.[14] The primary contribution to the degradation of k_{irr} is attributed to these loop defects acting as phonon scattering sites.

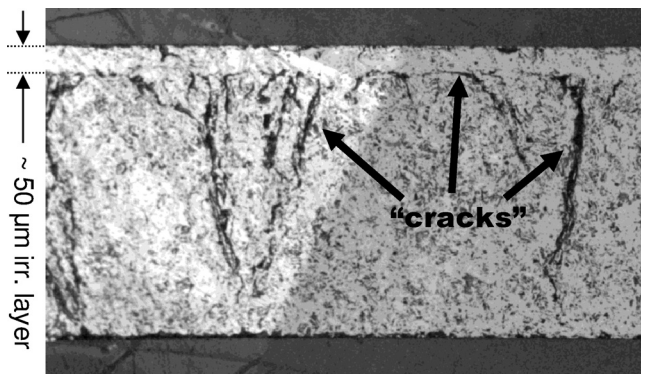

FIG. 7. Optical micrograph of irradiated-ZrC cross section. Irradiated layer has ~50 μm thickness. "Cracks" are clearly visible, terminating at depth of irradiation penetration. In some locations, showing evidence of having been pushed by proton front to form a boundary between the two zones.

V. SUMMARY AND CONCLUSIONS

Spatial scanning techniques of cross-sections prove valuable when combined with tomographic frequency scanning techniques. For the first time, such methodology has been applied to an irradiated sample. The methods complement and validate each other finding 55% degradation of thermal conductivity ($k_{irr} = 11.9\,W\,m^{-1}\,K^{-1}$ and $k_{ZrC} = 26.7\,W\,m^{-1}\,K^{-1}$) in ZrC irradiated to 1.75 dpa at 600 °C by a 2.6 MeV proton beam.

- Frequency scanning provides more straightforward thermophysical quantification but requires knowledge of the in-depth profile.
- SThM profiling provides good resolution for estimating irradiation penetration depth and relative characteristics of the profile.
- Possible artifact on R_{th} detection: the used spatial scanning methods involved excitation thermal gradients oriented parallel to the interface with R_{th} (unfavorable configuration for R_{th} detection); in the FD-PTR method, the R_{th} detection is based on the "reflection" of thermal waves traveling perpendicular to the interface with R_{th} (favorable configuration).

Spatial scanning PTR resolution is limited by heating spot size. Lock-in IRT is frequency limited, thus having thermal diffusion lengths too large for good spatial resolution, but has the advantage of quickly imaging the entire cross-section in a single measurement. SThM has the best resolution and gives a good approximation of the profile of thermal conductivity degradation. However due to difficulties associated with exact reproducibility of tip-sample contact conditions, it requires careful interpretation of results.

The proton-irradiated ZrC has a damage profile lending itself well to a discretely layered approximation used in FD-PTR. The damaged layer is $\sim 52 \pm 2\,\mu m$ thick with a relatively uniform thermal profile. A rather sharp transition to the virgin material was found at the back side of the radiation damaged layer. However, as evidenced by visual study and the tomographic profiles, a thermal resistance exists in the transition zone. Evidence suggests that the thermal resistance is due to the coalescence of void space driven by the proton irradiation front. The existence of such an effect merits further study.

Although SEM images and optical observation provide no indication of grain boundary separation, no irradiation-induced amorphization has been observed in similar ZrC samples.[14,39] Degradation of thermal conductivity in the irradiation-damaged zone is primarily attributed to the presence of a high concentration of Frank loops found in study of ZrC irradiated under similar conditions.[14]

The thermal transport measurement methodology used in this study can be expanded and applied to a more systematic study of ZrC irradiated by protons for a range of irradiation temperatures and dosages.

ACKNOWLEDGMENTS

Work by C.J. was performed using funding received from the DOE Office of Nuclear Energy's Nuclear Energy University Programs as well as the Chateaubriand Fellowship from the French Embassy in the U.S.

[1]G. Was, J. Busby, T. Allen, E. Kenik, A. Jensson, S. Bruemmer, J. Gan, A. Edwards, P. Scott, and P. Andreson, J. Nucl. Mater. **300**, 198 (2002).
[2]G. Was, *Fundamentals of Radiation Materials Science: Metals and Alloys* (Springer, New York, 2007).
[3]G. Was and T. Allen, in *Proceedings of the NATO Advanced Study Institute on Radiation Effects in Solids* (Springer-Verlag, Berlin, 2007), pp. 65–98.
[4]L. David, S. Gomès, G. Carlot, J. Roger, D. Fournier, C. Valot, and M. Raynaud, J. Appl. Phys. D **41**, 035502 (2008).
[5]J. Cabrero, F. Audubert, R. Pailler, A. Kusiak, J. Battaglia, and P. Weisbecker, J. Nucl. Mater. **396**, 202 (2010).
[6]K. Horne, H. Ban, A. Mandelis, and A. Matvienko, Mater. Sci. Eng. **177**, 164 (2012).
[7]R. Taylor and E. Storms, *Thermal Conductivity*, edited by P. G. Klemens and T. K. Chu (Plenum Press, New York, 1976), Vol. 14, pp. 161–174.
[8]W. Lengauer, S. Binder, K. Aigner, P. Ettmayer, A. Guillou, J. Debuigne, and G. Groboth, J. Alloy Compd. **217**, 137 (1995).
[9]Y. Ozaki and R. H. Zee, Mater. Sci. Eng. A: Struct. **202**, 134 (1995).
[10]M. L. Taubin, S. V. Fateev, M. V. Ivanov, and P. V. Shutov, Atom. Energy **70**, 55 (1991).
[11]L. L. Snead, Y. Katoh, and S. Kondo, J. Nucl. Mater. **399**, 200 (2010).
[12]E. F. Westrum, Jr. and G. Feick, J. Chem. Eng. Data **8**, 176 (1963).
[13]Y. S. Touloukian and E. H. Buyco, "Thermophysical properties of matter," *Specific Heat Nonmetallic Solids* (IFI/Plenum Press, New York, 1970), Vol. 5.
[14]Y. Yang, C. A. Dickerson, H. Swoboda, B. Miller, and T. R. Allen, J. Nucl. Mater. **378**, 341 (2008).
[15]J. F. Ziegler, J. P. Biersack, and M. D. Ziegler, *SRIM: The Stopping and Range of Ions in Matter* (SRIM Company, 2008).
[16]A. Majumdar, Annu. Rev. Mater. Sci. **29**, 505 (1999).
[17]L. Shi and A. Majumdar, "Micro-nano scale thermal imaging using scanning probe microscopy," *Applied Scanning Probe Methods*, edited by I. B. Bhushan, H. Fuchs, and S. Hosaka (Springer, Heidelberg, 2004), pp. 327–362.
[18]B. Cretin, S. Gomès, N. Trannoy, and P. Vairac, *Microscale and Nanoscale Heat Transfer*, edited by S. Volz (Springer, 2007), Vol. 107, pp. 181–238.
[19]C. Jensen, M. Chirtoc, J. Antoniow, and H. Ban, Int. J. Thermophys. **34**, 597 (2013).
[20]B. Cretin, Superlattice Microsyst. **35**, 253 (2004).
[21]G. Busse, D. Wu, and W. Karpen, J. Appl. Phys. **71**, 3962 (1992).
[22]M. Choi, K. Kang, J. Park, W. Kim, and K. Kim, NDT&E Int. **41**, 119 (2008).
[23]R. Montanini, Infrared Phys. Technol. **53**, 363 (2010).
[24]P.-E. Nordal and S. O. Kanstad, Phys. Scr. **20**, 659 (1979).
[25]R. Fuente, E. Apinaniz, A. Mendioroz, and A. Salazar, J. Appl. Phys. **110**, 033515 (2011).
[26]A. Salazar, R. Fuente, E. Apinaniz, A. Mendioroz, and R. Celorrio, J. Appl. Phys. **110**, 033516 (2011).
[27]M. Chirtoc, *Thermal Wave Physics and Related Photothermal Techniques: Basic Principles and Recent Developments*, edited by E. M. Moares (Transworld Research Network, Kerala, India, 2009), pp. 29–63.
[28]A. Mandelis, *Diffusion-Wave Fields: Mathematical Methods and Green Functions* (Springer, New York, 2001).
[29]D. Maillet, S. André, J.-C. Batsale, A. Degiovanni, and D. Maillet, *Thermal Quadrupoles: Solving the Heat Equation through Integral Transforms* (Wiley, Chichester, 2000).
[30]M. Chirtoc, J. Antoniow, J. Henry, P. Dole, and J. Pelzl, *Advanced Techniques and Applications on Scanning Probe Microscopy*, edited by F. Lei and J. L. Bubendorff (Transworld Research Network, Kerala, India, 2008), pp. 197–247.
[31]R. Taylor and J. Morreale, J. Am. Ceram. Soc. **47**, 69 (1964).
[32]Y. S. Touloukian, R. W. Powell, C. Y. Ho, and P. G. Klemens, "Thermophysical properties of matter," *Thermal Conductivity Nonmetallic Solids* (IFI/Plenum Press, New York, 1970), Vol. 2.
[33]E. K. Storms and P. Wagner, High Temp. Sci. **5**, 454 (1973).
[34]C. W. Lee, J. Nucl. Mater. **108–109**, 678 (1982).
[35]D. R. Clarke, Surf. Coat. Technol. **163–164**, 67 (2003).
[36]L. W. Hobbs, F. W. Clinard, S. J. Zinkle, and R. C. Ewing, J. Nucl. Mater. **216**, 291 (1994).
[37]Y. Yang, C. A. Dickerson, and T. R. Allen, J. Nucl. Mater. **392**, 200 (2009).
[38]L. Van Brutzel and J. Crocombette, Nucl. Instrum. Methods B **255**, 141 (2007).
[39]J. Gan, Y. Yang, C. Dickson, and T. Allen, J. Nucl. Mater. **389**, 317 (2009).